

Above-threshold-ionization structures in photoelectron momentum distributions for single ionization of He by a strong electromagnetic field

I. A. Ivanov* and A. S. Kheifets

*Research School of Physical Sciences and Engineering, The Australian National University, Canberra,
Australian Capital Territory 0200, Australia*

(Received 12 October 2009; published 8 December 2009)

Our numerical calculations support a recently advanced hypothesis that an individual photon absorption is still a valid concept in the tunneling regime of atomic ionization in a strong electromagnetic field. We observe characteristic structures in the photoelectron momentum distribution resulting from single ionization of the helium atom in the tunneling regime which are normally associated with above threshold ionization (ATI). The nodal structure of these ATI-like rings varies with the photon energy which can be attributed to altering parity of the photon numbers producing the corresponding rings.

DOI: [10.1103/PhysRevA.80.063418](https://doi.org/10.1103/PhysRevA.80.063418)

PACS number(s): 32.80.Rm, 32.80.Fb

I. INTRODUCTION

The well-known Keldysh theory [1] outlines two essentially different regimes of atomic ionization by strong electromagnetic (EM) fields. The atom is ionized either through tunneling or multiphoton ionization processes depending on the value of the Keldysh parameter $\gamma = \omega\sqrt{2I}/F$. This dimensionless parameter is expressed via the photon energy ω , the EM field strength F and the atomic ionization potential I , all the quantities are measured in atomic units. For values $\gamma < 1$, ionization proceeds through tunneling which is characterized by strong (exponential) dependence of ionization probabilities on the field strength. This implies that the ionization event occurs predominantly at the moments of the peak intensity of the EM field which is utilized in the so-called ADK model [2] of tunneling ionization. This model predicts a smooth distribution of the photoelectron momenta which is sharply centered at the point corresponding to zero momentum. The ADK theory provides a basis for theoretical description of various strong field ionization phenomena such as high harmonics generation [3,4] or formation of ultrashort pulses of EM radiation [5]. The ADK theory and its variations do not use the concept of an individual photon.

For values $\gamma > 1$, the multiphoton ionization process takes place which is characterized by appearance of sharp structures in electron spectra due to absorption of various numbers of individual photons from the field. For example, electron energy spectra in the domain of the multiphoton ionization show sequence of peaks separated by the photon energy, which are known as the above threshold ionization (ATI) peaks [6].

Experiments performed up until recently seem to have confirmed this clear separation of the tunneling and multiphoton regimes of strong field atomic ionization. This separation, however, was challenged in high-resolution measurements of photoelectron momentum distribution from noble gas atoms [7,8]. Typical values of the Keldysh parameter γ in these experiments were around 0.5. Yet, it was found that electron spectra, especially the electron distribution with the

momentum component P_z parallel to the polarization axis of the EM field, revealed the ATI-like structures.

In strong contradiction to the ADK model which predicts a smooth Gaussian profile for this distribution, the experiment [7] revealed a double-peak structure with a minimum at $P_z=0$. The authors of Ref. [7] suggested that their results could be explained by a process of resonantly enhanced ionization. Another explanation was proposed on the basis of the Coulomb-phase modification of the Keldysh-Faisal-Reiss theory [9] within the concept of individual photon absorption. In this work and the subsequent paper [10], the authors suggested that for a long enough pulse and correspondingly small bandwidth, no matter what actual value of γ is, the mechanism of absorption of individual photons is always at work.

In Refs. [11,12], it was suggested that this manifestation of the multiphoton effects deep in the tunneling regime was made possible by the long-range Coulomb potential effect, present in the case of single ionization of a neutral atom. In the paper [12], the authors identified appearance of these structures with a particular term of the S -matrix expansion which described interaction between the core and the ionized electron. The authors found that when this term was taken into account and averaging over the experimental field intensity was performed, they could satisfactorily reproduce distributions found in the experiment [7]. The effect of the atomic potential and the pulse duration on the double-peak structure of the longitudinal momentum distribution was studied in Ref. [13]. Using various model potentials and different pulse lengths, the authors found that for a long enough pulse the multiphoton effects were responsible for the appearance of the double-peak structure. On the other hand, for short two-cycle pulses it was the interaction of the outgoing electron and the atomic core that produced the double hump structure in the spectrum. In Ref. [14], it was found, that the double-peak structure in the longitudinal momentum distribution could be explained for short pulses using purely semiclassical notions of the ADK theory, without introducing the multiphoton effects if the Coulomb force acting on the electron after tunneling is taken into account.

In the present paper we continue these theoretical studies of the electron momentum distributions following the one-

*Corresponding author; igor.ivanov@anu.edu.au

electron ionization of helium in the tunneling regime. Our studies are based on numerical solution of the three-dimensional time-dependent Schrödinger equation (TDSE) with the Hartree-Fock potential of the helium atom. Results of Ref. [12] show that the structures arising in the longitudinal momentum distribution are, in fact, multipeak structures. However, less prominent peaks disappear after the focal volume averaging is performed. We show, that these substructures can be identified with the remains of the ATI rings present in the electron spectra for nonzero values of the transverse (perpendicular to the polarization axis) component of electron momentum. This result supports the hypothesis put forward in Ref. [9] that individual photon absorption can be identified even deep into the tunneling regime. Moreover, we find that the structure of these ATI-like rings exhibits rather sensitive dependence on the photon energy which is reminiscent to what one would expect for the process of multiphoton ionization.

The paper is organized as follows. In the next section we outline the formalism. In Sec. III we describe the numerical procedure we use and various checks we performed to test its accuracy. In Sec. IV we discuss the results.

II. THEORY

We seek a solution of the TDSE for a two-electron atom

$$i \frac{\partial \Psi}{\partial t} = \hat{H} \Psi, \quad (1)$$

with

$$\hat{H} = \hat{H}_{\text{atom}} + \hat{H}_{\text{int}}(t), \quad (2)$$

where

$$\hat{H}_{\text{atom}} = \frac{\hat{p}_1^2}{2} + \frac{\hat{p}_2^2}{2} - \frac{2}{r_1} - \frac{2}{r_2} + \frac{1}{|\mathbf{r}_1 - \mathbf{r}_2|}. \quad (3)$$

Interaction of the atomic system and the external EM field is written in the velocity gauge,

$$\hat{H}_{\text{int}}(t) = \mathbf{A}(t) \cdot (\hat{p}_1 + \hat{p}_2). \quad (4)$$

The vector potential is related to the ac field $\mathbf{F}(t) = f(t)\mathbf{F}_0 \cos(\omega t + \phi)$, where ω is the carrier frequency and ϕ is the carrier envelope phase (CEP), via $\mathbf{A}(t) = -\int_0^t \mathbf{F}(\tau) d\tau$. The function $f(t)$ describing envelope of the pulse is chosen in such a way that the amplitude of the ac field remains constant during the time interval $(T, T_1 - T)$, where $T = 2\pi/\omega$ is a period of the ac electromagnetic field, T_1 —total duration of the pulse. The field is ramped on and off smoothly over one ac field period. The ac electric field is assumed to be linearly polarized along the z axis.

In the interaction Hamiltonian given by the Eq. (4) we have omitted the $A^2(t)$ term present in the minimal coupling Hamiltonian describing atom-EM field interaction. This term can always be removed through a gauge transformation [15]. This gauge transformation amounts to the absorption of this term as a phase factor in the wave function. As long as we rely on the dipole approximation where vector potential is

spatially independent, this factor is unimportant, since it does not affect ionization probabilities. It should be taken into account, however, that use of the Hamiltonian given by the Eq. (4) instead of the minimal coupling Hamiltonian alters interpretation of the shift, which both continuum threshold and bound states undergo in the presence of the EM field. Hamiltonian (4) without the $A^2(t)$ term does not shift the continuum threshold. Instead, bound states energy levels are shifted downwards by an additional amount [15]. Total energy required to ionize the atom remains of course the same irrespective of the form of the interaction Hamiltonian which we use.

The solution of the TDSE is represented in the form of the basis set expansion,

$$\Psi(\mathbf{r}_1, \mathbf{r}_2, t) = \sum_j a_j(t) (1 + \hat{P}_{12}) \mathcal{Y}^{j, l_2}(\hat{\mathbf{r}}_1, \hat{\mathbf{r}}_2) f_{n_1 l_1}(r_1) f_{n_2 l_2}(r_2), \quad (5)$$

where \mathcal{Y} is a bipolar harmonic function [16], operator $1 + \hat{P}_{12}$ ensures proper symmetrization of the wave function, the index j is used as a shortcut for the set n_1, l_1, n_2, l_2, J specifying a basis vector. Radial orbitals f_{nl} in Eq. (5) were obtained by diagonalization of the target Hamiltonian [i.e., the Hamiltonian of the hydrogenlike ion with the same Z as in Eq. (3)], using the set of B splines of the order $k=7$. More details about the radial orbitals are given in the next Section and in Refs. [17–19].

Our choice of the gauge to describe the atom-field interaction is motivated by the following consideration. The use of the velocity gauge in numerical studies of photoionization processes in the tunneling regime may offer computational advantages [20,21]. In particular, considerably smaller number of the angular momentum states can be deployed in Eq. (5) as compared to the case of the length gauge.

Substitution of Eq. (5) into the TDSE results in a set of coupled differential equations for the amplitudes a_j which are solved by means of the Crank-Nicholson method [22] on the time interval $(0, T_1)$, where T_1 (typically 10 optical cycles) is total duration of the pulse.

The solution is then projected on the set of the field free singly-ionized atomic states. The set, which we use is provided by the so-called convergent close coupling (CCC) method [23,24], which gives us a solution of the problem of the electron scattering on a hydrogenic ion with the nuclear charge Z in the target state n_0, l_0, m_0 . Since we consider ionization without excitation, we have therefore $n_0=1$ and $l_0 = m_0=0$.

The CCC scattering wave function with the ingoing boundary conditions can be written as

$$\begin{aligned} \Psi_k^{(-)}(\mathbf{r}_1, \mathbf{r}_2) = & \sum_{lm} \Psi_{n_0 l_0 j k}^{(-)}(r_1, r_2) i^l e^{-i\delta_l^{(k)}} \\ & \times \langle l m l_0 m_0 | J M \rangle Y_{l_0 m_0}(\hat{\mathbf{r}}_1) Y_{lm}^*(\hat{\mathbf{r}}_2) Y_{lm}(\hat{\mathbf{k}}). \end{aligned} \quad (6)$$

The radial functions $\Psi_{n_0 l_0 j k}^{(-)}(r_1, r_2)$ are obtained by solving the Lippmann-Schwinger equations describing the scattering process. This set can be solved, in principle, for any number

of coupled channels. However, as we are dealing with the single ionization problem within the frozen core approximation, we can restrict the scattering problem to a one-channel calculation leaving the He^+ ion in its ground state.

Aided by this projection technique, we can compute electron distributions of interest. As we shall see, for the correct interpretation of these spectra it may be necessary to take into account the shifts of the energy levels due to interaction of the atom with the EM field. In the picture using the minimal coupling Hamiltonian, the dominant part of this shift is the shift of the continuum limit, which for long enough pulses is given by the ponderomotive energy $U_p = F_0^2/4\omega^2$ [25]. For the low frequency EM fields this shift can be quite significant and may far exceed the photon energy. As we mentioned above, in the picture using the Hamiltonian given by the Eq. (4), continuum limit does not shift, instead the ground state acquires additional downward shift, which for long pulses is equal to U_p . For the pulses of several optical cycles, which we consider below, the total shift of ground state (and the decay rate Γ) can be computed from the solution of the TDSE as follows [26]:

$$\Delta E - i\frac{\Gamma}{2} = \frac{1}{T_1} \int_0^{T_1} \frac{\langle \Phi(\tau) | \hat{H}_{\text{int}} | \Psi(\tau) \rangle}{\langle \Phi(\tau) | \Psi(\tau) \rangle} d\tau, \quad (7)$$

where $\Phi(t) = e^{-iE_0 t} \Phi_0$ is the ground state wave function, $\Psi(t)$ is the solution of TDSE, \hat{H}_{int} , given by the Eq. (4), describes the atom-field interaction and integrals are computed over the interval $(0, T_1)$ of the duration of the pulse.

III. NUMERICAL DETAILS

The set of the B splines used to construct the radial functions in Eq. (5) was chosen as follows. The knots defining the splines were located at the sequence of points lying in $[0, R_{\text{max}}]$ where the size of the box R_{max} was 400 a.u. All the knots t_i were simple ones except for the knots located at the origin and the outer boundary $R = R_{\text{max}}$ of the box. These knots had multiplicity $k=7$. The simple knots were distributed uniformly in $(0, R_{\text{max}})$ (approximately 200 B splines were employed for each l). For each value of the angular momentum l the first $l+1$ B splines and the last B spline resulting from this sequence of knots were discarded. The omission of first $l+1$ B splines ensured that any B spline in the set decreased as r^{l+1} (or faster) at the origin, the omission of the last B spline ensured that all B splines of a set assumed the zero value at the outer boundary.

We used this recipe in previous works [17–19] for calculations of one- and two-photon ionization of two-electron systems. Present problem of ionization by low frequency ac field differs in the respect, that we have to include many more angular momenta [both in Eq. (5) and in the CCC expansion (6)]. To describe accurately ATI processes in the velocity gauge, angular momenta of up to 10 are to be included in the calculation [20]. It is this upper limit that we used both for l_1, l_2, J in Eq. (5) and l, J in Eq. (6).

To make the problem tractable numerically, we had to impose some additional restrictions on the basis set in Eq. (5). Since we are interested in one-electron ionization, we

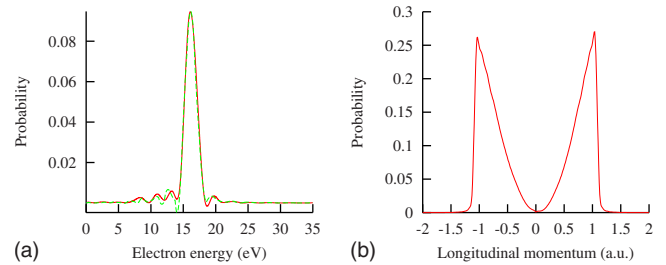


FIG. 1. (Color online) Electron distributions for single ionization of helium with the following field parameters: $\omega=40$ eV, $T_1=20T$, $F_0=0.1$ a.u. Left panel: energy distribution, solid (red) line projection on CCC states, dashed (green) line-projection on helium pseudostates. Right panel: distribution as function of longitudinal (along polarization of the EM field) component of the momentum.

may “freeze” (either completely or partially) one of the electrons in Eq. (5), restricting the number of angular momentum and radial states for this electron. Natural (and apparently harmless) restriction for helium is to freeze one of the electrons completely, i.e., allow this electron to occupy only the $1s$ state of the target ion. As long as we are interested in ionization of atom by the infrared radiation, this restriction of the basis set introduces only a minor error in the computed ionization probabilities (of the order of a percent) [27]. This fact can be understood if we take into account that a typical value of the electron excursion radius for the infrared radiation of large intensity far exceeds the size of the parent ion. It is not surprising, therefore, that ionization in this case is not very sensitive to the fine details of the atomic structure. Yet, even with this restriction, and the B spline basis set described above, we can get a reasonably accurate value of -2.87230 a.u. for the ground-state energy of helium.

To give an illustration of our computational procedures, we consider a simple case of ionization of the helium atom by a 40 eV VUV photon. This is a simple problem, for which almost exact answer for the ionization probability can be obtained [28] and we can use it to check the accuracy of our procedure. In particular, we can check the effect which the restriction of the basis set by freezing the state of one of the electrons, may have on the results. As we noted above, we may expect, that ionization by the infrared radiation would show less sensitivity to the atomic structure than we can expect for the ionization by a 40 eV VUV photon. If we find that our basis set gives accurate enough results in the latter case, we may expect it to be yet more accurate in the former.

In Fig. 1 we show the electron energy distribution (left) and the longitudinal momentum distribution (right) for the single ionization of helium with the following field parameters: $\omega=40$ eV, $T_1=20T$, $F_0=0.1$ a.u.

To compute the distributions shown in Fig. 1, the basis set [Eq. (5)] was restricted by freezing one of the electrons to the $1s$ state of the He^+ ion. By integrating either the energy or momentum distributions (the answers are identical within a fraction of a percent), we can compute the total ionization probability after the end of the 20-cycle pulse. This probability turns out to be $P_{\text{ion}}=0.255$. The ionization probability is related to the decay rate via $P_{\text{ion}}=1-e^{-\Gamma T_1}$, where T_1 is duration of the pulse. Thus produced $\Gamma=3.67 \times 10^{-3}$ a.u. can

be compared with the value $\Gamma=4.21 \times 10^{-3}$ a.u. obtained from a highly accurate Hylleraas basis calculation with a complete account of the electron correlations [28]. The Γ value obtained in the present TDSE calculation can be relatively easily improved by relaxing the frozen $1s$ orbital. For example, by adding the $2p$ ionic state to the basis (5) we obtain the Γ value accurate within 3%. This is not, however, the point of the present demonstration. What we meant to demonstrate was the adequacy of the frozen core $1s$ calculation which could provide a reasonably accurate description of single ionization of He by 40 eV photons. As we discussed above, we may expect accuracy to improve for lower energy photons.

This demonstrative calculation also allows us to check other ingredients of our numerical scheme. On the left panel of Fig. 1 we show (solid line) results of the projection of the solution of TDSE on the manifold of the CCC states. Because single ionization is by far the dominant channel, we may use alternative way of computing the energy spectrum, based on the concept of the pseudostates [29] of a two-electron system. To compute the probability of ionization within a given energy range we need to be able to calculate the projection operator on the part of the continuum spectrum of the two-electron atom, corresponding to this energy range. One way to compute such a projection operator is to use explicit set of the scattering states, for example the CCC states which we use in the present work. Alternative way is to diagonalize the helium Hamiltonian in a box, produce a set of densely spaced (but discrete) levels, and use this set to build the projection operator. In other words, the set thus obtained provides the discretized representation of the projection operator (and related quantities, such as resolvent operator) [29]. We followed this recipe by diagonalizing the helium Hamiltonian using the same basis set as we used to solve the TDSE. Results (dashed green line on the left panel) are virtually identical to the results obtained if we use the manifold of the CCC states. What this tells us is that the continuum spectrum of helium viewed by the CCC method, and the continuum spectrum of helium as rendered by the basis we use in Eq. (5) nearly coincide. More formally, if \hat{P}_{CCC} is the projection operator on the part of the continuum spectrum of He constructed using the CCC basis, and \hat{P}_{TDSE} is the same operator constructed using the basis (5), then $\hat{P}_{\text{TDSE}} \approx \hat{P}_{\text{CCC}}$. This is a nontrivial result since the basis we use and the basis used in the CCC method are different. This result guarantees that when we compute ionization probabilities by projecting solution of TDSE on the manifold of the CCC state, we do not introduce a significant error. This is an important conclusion. While we could, in principle, calculate the energy spectrum using the discretized representation of the continuum spectrum for low frequencies, the projection on the CCC states (or some equivalent basis) is the only way to obtain the momentum distributions such as the one shown on the right panel of Fig. 1.

To conclude discussion of this test calculation, we should mention an alternative way to compute Γ which is based on Eq. (7). Calculation using this formula gives essentially the same value for the decay rate $\Gamma=3.55 \times 10^{-3}$ a.u.

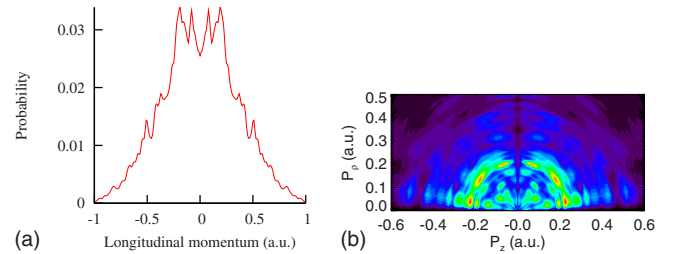


FIG. 2. (Color online) Photoelectron momentum distribution from single ionization of helium. Laser field parameters: $\omega = 1.56$ eV, pulse duration 10 optical cycles, intensity 6×10^{14} W/cm², the Keldysh parameter $\gamma=0.58$. Left panel: electron distribution with respect to the longitudinal momentum. Right panel: 2D distribution (logarithmic scale) as function of the momentum components in the cylindrical coordinates.

IV. RESULTS

We open this section by presenting our results obtained for a 10 optical cycle pulse with the carrier frequency corresponding to 1.56 eV photon energy. These laser field parameters were used in the experimental work [7] where the ATI-like pattern in the photoelectron momentum distribution was observed in the tunneling regime. Similarly to work [13], we average the results of the TDSE calculation over the phase ϕ . More specifically, for each set of the field parameters reported below, we perform computations with ten values of CEP distributed uniformly on the interval $(0, \pi)$ and average the obtained spectra over this set.

There is a second type of average associated with the laser field intensity distribution over the focal volume. This averaging is known to further smooth the theoretical electron spectra [12]. We do not perform this averaging, since we are specifically interested in the features in the photoelectron spectra which survive the CEP average, but are smoothed out by the focal volume average. These additional features, which may not be seen experimentally, provide yet another evidence of the “multiphoton” origin of the ATI-like structures.

In Fig. 2 we present the electron momentum distributions corresponding to the field intensity of 0.6 PW/cm². The same field intensity was used both in the experimental work [7] and theoretical paper [12]. The right panel of Fig. 2 shows the two-dimensional (2D) electron distribution $Q(P_z, P_\rho)$ as a function of the momentum components in the cylindrical coordinates with the z axis directed along the polarization axis of the light. The left panel of this figure shows the ionization probability as a function of the longitudinal component P_z only. The latter is computed as an integral: $\int_0^\infty Q(P_z, P_\rho) dP_\rho$.

The longitudinal momentum distribution displayed on the left panel of Fig. 2 shows the two highest maxima located at $\pm P_z \approx 0.2$ a.u., and the smaller maxima at $\pm P_z \approx 0.4$ a.u. and $\pm P_z \approx 0.5$ a.u. The origin of these peaks can be explained as follows [9]. Even deep in the tunneling regime (present value of the Keldysh parameter $\gamma=0.58$), the sharp structures in the photoelectron spectra can still be associated with absorption of the integer number of photons. This can be done using the conventional energy conservation formula

$E = N\omega - I - U_p$, where I is the ionization potential, the ponderomotive potential U_p accounts for the shift of the continuum, N is an integer such that the kinetic energy E is positive. It was argued in Ref [9]. that, in the tunneling regime, the electron cannot acquire large momentum P_ρ perpendicular to the polarization axis. Hence, one may express the kinetic energy as $E \approx P_z^2/2$ and, consequently, the positions of the peaks in the electron longitudinal momentum distribution correspond to $P_z \approx \sqrt{2(N\omega - I - U_p)}$. This reasoning explains the main features of the phenomenon such as appearance of two sequences of peaks located symmetrically with $P_z=0$, the cusplike structure of the peaks, and the spacing between the consecutive peaks in the spectrum.

In the above formulas it was understood that the change of the ionization potential due to the presence of the EM field is given by the ponderomotive energy U_p . If we are interested in determining the exact value of N responsible for the appearance of a particular peak in the spectrum, then we must take into account the total shift of the energy of ground state given by the Eq. (7). This shift is largely dominated by the quantity $-U_p$, so that $\Delta E = -U_p + \Delta E_1$, where ΔE_1 is small comparing to the ponderomotive energy [we remind, that in the picture rendered by the Hamiltonian given by the Eq. (4) ionization threshold does not shift, instead bound states are shifted downwards]. Account of the additional shift ΔE_1 , however, proves to be important. For the very low photon frequencies we consider, even this small shift can be larger than photon energy. For the pulse parameters we consider, for instance, calculation according to Eq. (7) gives for the total shift of the ground state $\Delta E = -41.14$ eV, and $U_p = 35.52$ eV.

The above formula for the location of the peaks in the longitudinal momentum distribution, which we should now write as $P_z \approx \sqrt{2(N\omega - I + \Delta E)}$, gives the following peak positions: 0.22 a.u. ($N=42$), 0.40 a.u. ($N=43$), 0.53 a.u. ($N=44$). We used the ionization potential $I = 0.872$ a.u. corresponding to the ground-state energy obtained with our basis. The peak nearest to $P_z=0$ in Fig. 2 is thus due to absorption of 42 photons. Note, that the additional correction ΔE_1 to the shift of the ground state plays an important role here. If we did not use this correction we would have obtained a sequence 0.04 a.u. ($N=38$), 0.34 a.u. ($N=39$), 0.48 a.u. ($N=40$) which agrees considerably worse with the observed positions of the peaks displayed in Fig. 2. Thus, we get better agreement with the observed position of the peaks and, more importantly, more accurate estimate of the number of photons which are responsible for appearance of these peaks. This circumstance is rather important because it allows us to get a glimpse of the behavior of electron distribution for nonzero values of the transverse momentum P_ρ .

As one can see from the plot on the left panel of Fig. 2, the peaks nearest to $P_z=0$ are split. Such splitting has also been found in the calculation [12]. The origin of this splitting is clear from the plot on the right panel of Fig. 2. This plot shows that the ionization probability has several maxima lying on a circle with the radius approximately equal to 0.23 a.u. in the (P_z, P_ρ) plane. One can clearly discern six such maxima. In each quadrant the two maxima nearest to the P_z axis (at $P_z \approx \pm 0.22$ a.u., $P_\rho \approx 0.03$ a.u. and $P_z \approx \pm 0.16$ a.u., $P_\rho \approx 0.16$ a.u.) have comparable intensities.

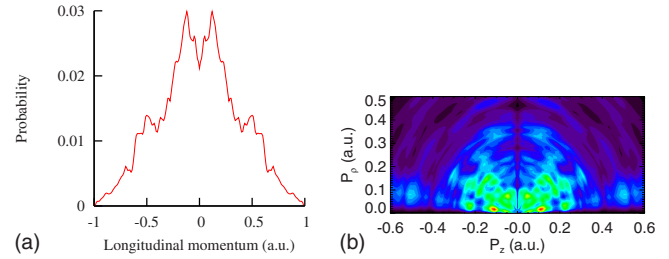


FIG. 3. (Color online) Same as Fig. 2 for the photon energy $\omega = 1.63$ eV.

The maxima lying farther away from the P_z axis (those with $P_z \approx \pm 0.03$ a.u. and $P_\rho \approx 0.22$ a.u.), are notably weaker.

This circular nodal structure, which is reminiscent of the multiphoton ATI rings, can be interpreted as remnants of the ATI ring in the (P_z, P_ρ) plane. The maxima with the largest values of P_ρ are weaker since in the tunneling regime ionization proceeds predominantly into the states with small transversal momenta. After the P_ρ integration, this nodal structure of the 2D distribution results in the additional splitting of the main peaks near $P_z=0$ on the plot displayed on the left panel of Fig. 2.

We cannot expect to see all the details which one would see for a truly multiphoton ionization corresponding to absorption of 42 photons. In the tunneling regime, the ATI structures, if present, are expected to be considerably distorted. Nevertheless, the structure observed on the 2D plot of Fig. 2 is suggestive of the angular pattern characteristic to the multiphoton ionization.

If this interpretation is correct, we can expect the probability distribution along the ATI ring to depend on the parity of the photon number which correspond to the ring. In the pure multiphoton case the transition amplitudes which produce the 2D distributions corresponding to absorption of even and odd number of photons would be expressed as linear combinations of Legendre polynomials of even and odd degree $P_l(\theta)$, correspondingly. Odd degree Legendre polynomials have nodes at $\theta = \pi/2$ corresponding to the P_ρ axis of the 2D plot of Fig. 2. We can expect, therefore, to see less structure near this axis in the case of the ATI ring corresponding to an odd number of absorbed photons.

The ring corresponding to the odd number of absorbed photons in Fig. 2 is too dim to make any conclusions. We performed therefore a separate calculation of single-electron ionization of helium for the same intensity and slightly shifted frequency $\omega = 1.63$ eV. A calculation analogous to the one given above for $\omega = 1.56$ eV, shows that for this shifted frequency the minimum number of photons needed to ionize the helium atom is odd ($N=39$). The results of this calculation are summarized in Fig. 3. One can see that, in agreement with our expectations, much less structure is visible in the 2D distribution away from the P_z axis. We should emphasize that the field parameters in these two cases are very close. The total ionization probabilities, therefore, differ only slightly, as can be observed from the plots on left panels of Figs. 2 and 3. As one can see, both height and widths of the longitudinal distributions are nearly the same. What is different is the absence of the splitting of the main peaks on

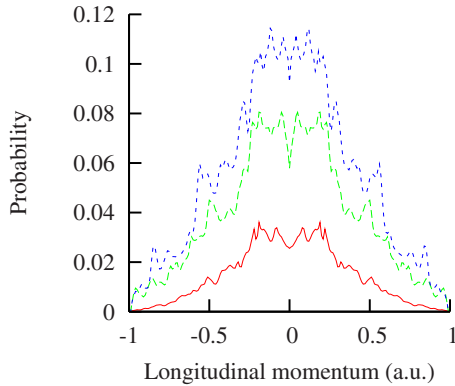


FIG. 4. (Color online) Photoelectron momentum distribution from single ionization of helium. Laser field parameters: $\omega = 1.56$ eV, pulse duration 10 optical cycles. Intensities: 6×10^{14} W/cm², red (lower) curve; 10^{15} W/cm², green (middle) curve; 2×10^{15} W/cm², blue (upper) curve.

the plot on the left panel of Fig. 3. We interpret this difference as due to the difference in the 2D probability distributions on the ATI rings nearest to the origin. As we suggested, this difference can be linked to the different parities of the photon numbers needed to produce these structures.

The split structure of the peaks is present for higher intensities as well. We performed calculations for the set of intensities reported in the experimental paper [7]. Results for longitudinal momentum distributions are shown in Fig. 4.

V. CONCLUSION AND FURTHER DIRECTIONS

We studied the process of single-electron ionization of helium by the laser field with the set of parameters identical to the experimental work [7]. In this work, a double-peak structure in the longitudinal momentum distribution was observed for the first time. This structure was later explained as originating from the absorption of an integer number of photons from the laser field deep in the tunneling regime [9]. This absorption also produces the local maxima in the corresponding 2D distributions with nearly zero P_ρ and P_z defined by the energy conservation. It was conjectured in Refs. [9,10] that the mechanism of absorption of individual photons is present even deep in the tunneling regime.

We report additional evidence in favor of this hypothesis. Our study of 2D momentum distributions shows, that traces of the ATI structures can be discerned even farther away from the P_z axis, making it almost a true ATI ring. Moreover, there are indications, that these structures are very sensitive to the photon frequency, which can be interpreted as manifestation of different nodal structures of ATI rings for different parities of photon numbers producing the rings.

These structures in the 2D momentum distributions present for nonzero values of transverse momentum manifest themselves as multipeak structures in the longitudinal momentum distributions. It is clear, that these structures are rather fragile.

As was shown in [12], where the multipeak structure in the longitudinal momentum distribution was also found, the average over the focal volume smoothes out the distributions. It is easy to give at least one reason why variations of intensity in the laser focus may produce this effect. For the present case of low photon frequencies and large ponderomotive energy, relatively small change of the field parameters may change the ionization threshold, and consequently the nodal structure of the ATI-like ring, producing considerable change in the distributions as comparison of Figs. 2 and 3 shows. Experimentally, therefore, the multipeak structures in the longitudinal momentum distributions may be difficult to observe, requiring uniform spatial distribution of intensity in the focal volume.

We did not try to simulate the effects of the nonuniform spatial distribution of the EM field intensity in our paper. Computational procedure which we adopt in the present work relies on the numerical solution of the fully dimensional TDSE for the realistic model of the helium atom. Averaging over the spatial distribution of the EM field intensity would necessitate multiple solutions of the TDSE with various field parameters. The average over the CEP distribution, which we do perform, implies that, for a given field intensity, we have to solve TDSE ten times with various CEP values for the driving pulse. Additional averaging over different field intensities would have put a considerable stress on our computational resources. The point we wished to make in the paper was, however, not so much the feasibility of the experimental observation of the multipeak structure in the longitudinal momentum distributions. We tried to demonstrate its existence in the electron spectra for the field of constant amplitude, which, to our opinion, is another unexpected manifestation of the multiphoton mechanism working deep in the regime of tunneling ionization.

In the future, we would like to extend the computational scheme used in the present work to double ionization of helium by a strong laser field in the tunneling regime [30]. Computationally, this is a rather challenging problem which requires to propagate in time an atomic system with two active electrons. However, we can concentrate specifically on the rescattering mechanism of the nonsequential double ionization [3] which is known to be a dominant mechanism of this process [31]. In this mechanism, only one atomic electron is tunneled out and, on revisiting the nucleus, it knocks out the second electron. To describe such a scattering process, we can use the present computational scheme replacing the CCC wave function of the singly-ionized scattering state by the corresponding CCC wave function describing the doubly ionized continuum.

ACKNOWLEDGMENTS

The authors acknowledge support of the Australian Research Council in the form of the Discovery Grant No. DP0771312. Resources of the National Computational Infrastructure (NCI) Facility were employed.

- [1] L. V. Keldysh, Zh. Eksp. Teor. Fiz. **47**, 1945 (1964) [Sov. Phys. JETP **20**, 1307 (1965)].
- [2] N. B. Delone and V. P. Krainov, J. Opt. Soc. Am. B **8**, 1207 (1991).
- [3] P. B. Corkum, Phys. Rev. Lett. **71**, 1994 (1993).
- [4] M. Lewenstein, P. Balcou, M. Y. Ivanov, A. L'Huillier, and P. B. Corkum, Phys. Rev. A **49**, 2117 (1994).
- [5] P. Antoine, A. L'Huillier, and M. Lewenstein, Phys. Rev. Lett. **77**, 1234 (1996).
- [6] P. Agostini, F. Fabre, G. Mainfray, G. Petite, and N. K. Rahman, Phys. Rev. Lett. **42**, 1127 (1979).
- [7] A. Rudenko, K. Zrost, C. D. Schroter, V. L. B. de Jesus, B. Feuerstein, R. Moshhammer, and J. Ullrich, J. Phys. B **37**, L407 (2004).
- [8] C. M. Maharjan, A. S. Alnaser, I. Litvinyuk, P. Ranitovic, and C. L. Cocke, J. Phys. B **39**, 1955 (2006).
- [9] F. H. M. Faisal and G. Schlegel, J. Phys. B **38**, L223 (2005).
- [10] F. H. M. Faisal and G. Schlegel, J. Mod. Opt. **53**, 207 (2006).
- [11] Z. Chen, T. Morishita, A.-T. Le, M. Wickenhauser, X. M. Tong, and C. D. Lin, Phys. Rev. A **74**, 053405 (2006).
- [12] L. Guo, J. Chen, J. Liu, and Y. Q. Gu, Phys. Rev. A **77**, 033413 (2008).
- [13] M. Abu-samha, D. Dimitrovski, and L. B. Madsen, J. Phys. B **41**, 245601 (2008).
- [14] K. I. Dimitriou, D. G. Arbó, S. Yoshida, E. Persson, and J. Burgdörfer, Phys. Rev. A **70**, 061401(R) (2004).
- [15] R. Shakeshaft and X. Tang, Phys. Rev. A **36**, 3193 (1987).
- [16] D. A. Varshalovich, A. N. Moskalev, and V. K. Khersonskii, *Quantum Theory of Angular Momentum* (World Scientific, Singapore, 1988).
- [17] I. A. Ivanov and A. S. Kheifets, Phys. Rev. A **74**, 042710 (2006).
- [18] I. A. Ivanov and A. S. Kheifets, Phys. Rev. A **75**, 062701 (2007).
- [19] I. A. Ivanov and A. S. Kheifets, Phys. Rev. A **75**, 033411 (2007).
- [20] E. Cormier and P. Lambropoulos, J. Phys. B **29**, 1667 (1996).
- [21] M. Nurhuda and F. H. M. Faisal, Phys. Rev. A **60**, 3125 (1999).
- [22] A. Goldberg, H. M. Schey, and J. L. Schwartz, Am. J. Phys. **35**, 177 (1967).
- [23] I. Bray, Phys. Rev. A **49**, 1066 (1994).
- [24] I. Bray and A. T. Stelbovics, Adv. At. Mol. Phys. **35**, 209 (1995).
- [25] H. G. Muller, A. Tip, and M. J. van der Wiel, J. Phys. B **16**, L679 (1983).
- [26] P. W. Langhoff, S. T. Epstein, and M. Karplus, Rev. Mod. Phys. **44**, 602 (1972).
- [27] H. W. van der Hart, B. J. S. Doherty, J. S. Parker, and K. T. Taylor, J. Phys. B **38**, L207 (2005).
- [28] I. A. Ivanov and A. S. Kheifets, Eur. Phys. J. D **38**, 249 (2006).
- [29] E. Cormier and P. Lambropoulos, J. Phys. B **28**, 5043 (1995).
- [30] A. Rudenko, V. L. B. de Jesus, T. Ergler, K. Zrost, B. Feuerstein, C. D. Schröter, R. Moshhammer, and J. Ullrich, Phys. Rev. Lett. **99**, 263003 (2007).
- [31] S. Micheau, Z. Chen, A.-T. Le, and C. D. Lin, Phys. Rev. A **79**, 013417 (2009).